


Preparation of magnetic-activated biocarbon composite from red algae for dye removal from water

Julinawati¹, Rahmi^{1*} , Zuhrah Putri Karnain¹, Irfan Mustafa¹,
Kartika MZ¹, Mutia Farida¹, Andriy Anta Kacaribu² 

¹ Department of Chemistry, Faculty of Mathematics and Natural Sciences, Universitas Syiah Kuala, Banda Aceh, 23111, Aceh, Indonesia

² Doctoral Program of Agricultural Science, Postgraduate School, Universitas Syiah Kuala, Banda Aceh 23111, Indonesia

* Corresponding author's email: rahmi@usk.ac.id

ABSTRACT

Magnetic-activated biochar (MAB) composite has been prepared from red algae and applied to remove methylene blue (MB) and Remazol brilliant yellow FG (RBY) dyes from water. The biocarbon prepared from red algae, following synthesized of magnetic biocarbon composites with nickel chloride hexahydrate ($\text{NiCl}_2 \cdot 6\text{H}_2\text{O}$) and activated using various concentrations of KOH. The adsorption efficiency (%E) of each MAB composite was examined. The MAB composite with the highest adsorption efficiency was used for the adsorption study with various contact times, pH, adsorbent masses/dosages, and initial concentrations of dyes. The MAB composite was characterized by Fourier transform infrared (FTIR), scanning electron microscopes (SEM), X-ray diffraction (XRD), and particle size analyzer (PSA). The MAB composite yielded optimal results in red algae: KOH ratio of 1: 0.5 (RA(Ni)0.5). The adsorption results showed that the optimum adsorption conditions for MB and RBY dyes occurred at pH 10 and 4, an adsorption time of 80 and 60 minutes, adsorbent dosages of 0.1 and 0.2 g, and adsorbate concentration of 35 mg/L with absorption efficiency (%E) of 95.99 and 89.94%, and adsorption capacity of 16.799 and 7.869 mg/L, respectively. The isotherm model for MB and RBY dye adsorption is the Freundlich isotherm ($R^2 = 0.9914$), and the Langmuir isotherm ($R^2 = 0.995$), respectively. Regeneration test revealed that the RA(Ni)0.5 composite is more efficient in adsorbing cationic dyes (MB – 83.02%) compared to anionic dyes (RBY – 67.08%) after 15 repetitions. The RA(Ni)0.5 composite was proven to have the potential as an adsorbent for the adsorption of MB and RBY dyes from water.

Keywords: red algae, composite, adsorption, isotherm, methylene blue and Remazol brilliant yellow.

INTRODUCTION

The growing industrialization, such as dyeing, textile, pulp, and paper production generate dye waste, which is discharged into waterways, causes severe in human and ecological health (Periyasamy, 2024). Dyes can cause various harmful effects, including generative chemical cystitis, digestive tract and skin irritation, respiratory and renal failure, ingestion may also lead to nausea, vomiting, diarrhea, as well as more severe conditions, such as methemoglobinemia, seizures, tachycardia, and dyspnea. These dyes contain various organic compounds and toxic

substances that harm fish and other aquatic organisms (Al-Tohamy et al., 2022; Lellis et al., 2019). Their presence in water sources is highly undesirable, not only due to environmental toxicity but also because of their strong visual pollution. Various methods have been used to treat the waste containing synthetic dyes, including biological, physical and chemical methods, such as adsorption, coagulation/flocculation, advanced oxidation (ozonation), and membrane filtration (Algarni and Al-Mohaimeed, 2022). Adsorption using an adsorbent is a method commonly used in the treatment of wastewater, because simple and high adsorption capacity (Fathana et al., 2023a).

Adsorbents from biomass have been widely used for wastewater treatment due to their large availability in the environment, such as cellulose (Fathana et al., 2023c), chitosan (Fathana et al., 2023b; Rahmi et al., 2017, 2023), polylactic acid from lactic acid (Kacaribu and Darwin, 2024), clay (Julinawati et al., 2023), activated carbon (Rahmi, 2018; Rahmi et al., 2018), algae (Buhani et al., 2021; Khan et al., 2023).

Algae constitute a group of marine plants often referred to as seaweed. Seaweed is a species of macroalgae consisting of green algae, brown algae, and red algae. Because of their widespread availability, affordability, and environmental friendliness (Hemavathy et al., 2025; Menaa et al., 2021; Prisa et al., 2024), algae have become a viable natural adsorbent for eliminating colors from textile wastewater (Abdel-Aziz et al., 2024). Their special makeup, especially the polysaccharide, protein, and lipid content—all essential for adsorption processes—makes them so powerful. The main constituents of red algal cell walls are polysaccharides, including agar, carrageenan, and alginate. These biopolymers are known for forming compounds with dyes via ion exchange, hydrogen bonding, and electrostatic interactions. Red algae's polysaccharides, for example, have been demonstrated in experiments to efficiently extract cationic and anionic dyes from aqueous solutions (Oualid et al., 2020; Fakhri et al., 2023). The high adsorption capacity of these polysaccharides is due to the presence of hydroxyl and carboxyl functional groups, which serve as active binding sites for dye molecules (Show et al., 2024; Yadav et al., 2022). This biomass can be utilized as biochar or biocarbon-based adsorbent to remove dyes from water and wastewater.

Several studies have highlighted the potential of marine macroalgae as natural adsorbents for removing hazardous dyes from aquatic environments. Boukarma et al. (2024) reported that three species of macroalgae – *Fucus spiralis*, *Ulva intestinalis*, and *Corallina officinalis*, demonstrated the ability to adsorb the toxic organic dye crystal violet (CV). Their findings revealed variations in the adsorptive properties of these algae, with *F. spiralis* adsorbing CV onto a homogeneous monolayer. At the same time, *U. intestinalis* and *C. officinalis* exhibited both homogeneous monolayer and heterogeneous multilayer adsorption. The predicted monolayer adsorption capacities at 25 °C were approximately

53, 55, and 97 mg/g for *F. spiralis*, *C. officinalis*, and *U. intestinalis*, respectively (Boukarma et al., 2024). Fazal et al. (2021) investigated the effectiveness of macroalgae-based biochar compared to coal-based biochar for removing MB from both simulated and real textile wastewater. Their findings demonstrated that both types of biochar could adsorb more than 90% of MB from simulated wastewater within 10 minutes, utilizing their active surface sites. Notably, macroalgae-based biochar exhibited a high % dye removal efficiency of 75% even in real textile wastewater and maintained 67% efficiency during the second regeneration cycle. Their finding noted that the maximum biosorption capacity of macroalgae-based biochar reached 353.9 mg/g (Fazal et al., 2021).

Composite-based adsorbents for water and wastewater treatment have been widely developed (Rahmi et al., 2021), with MAB composites gaining attention due to their high porosity, larger surface area, faster reactivity, and specific affinity for various pollutants, especially to dyes. Recent advancements in biocarbon from algae modification have further improved adsorption capabilities for organic pollutants. For instance, a magnetic biochar derived from *Ulva fasciata* marine algae (*Ulva fasciata* biochar, UFBC) modified with Fe_3O_4 (UFBC-MIO) has been developed to enhance adsorption performance. Studies have shown that UFBC-MIO effectively removes MB, achieving an adsorption capacity of 50.12 mg/g at pH 9 with a biochar dosage of 2 g/L (Kadimpati et al., 2024). The incorporation of magnetic materials such as Fe_3O_4 into algae-derived biocarbon composites is not only aimed at increasing adsorption efficiency, but also providing magnetic properties that simplify the separation and recovery of the adsorbent from aqueous systems. These magnetic properties allow for easy removal of the spent adsorbent using an external magnetic field, reducing secondary waste and enhancing the recyclability of the material. Moreover, the synergy between the porous structure of algae biochar and the surface activity of magnetic particles offers more accessible active sites, improving adsorption kinetics and capacity.

The synthesis of composites is expected to yield new materials with two primary properties: adsorption capability biocarbon from algae and magnetic properties from incorporated magnetic materials within the red algae structural network. Hence, this combination is rationalized

by the need for both high adsorption efficiency and operational practicality in dye-contaminated wastewater treatment. In this study, the magnetic property of the composite material is introduced using $\text{NiCl}_2 \cdot 6\text{H}_2\text{O}$. Nickel-based compounds are known for their paramagnetic behavior, which enables the synthesized biochar composite to respond to an external magnetic field. The presence of Ni^{2+} ions contributes to the development of magnetic domains within the structure, facilitating the magnetic separation of the adsorbent after wastewater treatment processes. Adding magnetic properties is anticipated to facilitate the active site, enabling a more efficient and rapid adsorption process using an external magnetic field. No literature has explored the development of MAB composites from Iboih Beach, Sabang City, Indonesia, red algae as recyclable dye adsorbents. Therefore, this study aimed to investigate the potential of Sabang marine red algae as a MAB-based adsorbent.

MATERIALS AND METHODS

Chemicals and reagents

The reagents and chemicals used in this study were nickel (II) chloride hexahydrate ($\text{NiCl}_2 \cdot 6\text{H}_2\text{O}$), potassium hydroxide (KOH), hydrochloric acid

(HCl), sodium hydroxide (NaOH), Methylene blue, and Remazol brilliant yellow FG (RBY) dyes purchased from Sigma-Aldrich (Singapore) (analytical grade), as well as distilled water.

Preparation of red algae

The red algae used in the present study were obtained from a local algae farmer in Iboih Beach, Sabang City, Indonesia (coordinates $5^\circ 53' 20.6''$ N $95^\circ 16' 38.3''$ E). The Oceanography Laboratory of the Badan Riset dan Inovasi Nasional (BRIN) Research Centre, Ancol, North Jakarta, was used to determine the taxonomy of red algae samples. The taxonomy or herbarium analysis of the red algae used in this study is classified as follows:

- kingdom: plants,
- division: Rhodophyta,
- class: Florideophyceae,
- order: Ceramiales,
- family: Delesseriaceae,
- genus: *Acrosorium*,
- species: *Acrosorium flabellatum*.

The red algae species used in present studies is *Acrosorium flabellatum*, this raw material was used to development of composited based adsorbent to removal dyes pollutants from water. The sample used were depicted in Figure 1.



Figure 1. Photograph of: wet (A), after cleaning (B), dried (C), and dried powder (D) of red algae biomass

Preparation of red algae MAB composites

Red algae were washed with distilled water until clean, dried at 80 °C for 48 hours, and crushed into powder. Then, 40 g of red algae powder was soaked with 400 mL of 0.5 M $\text{NiCl}_2 \cdot 6\text{H}_2\text{O}$ solution for 24 hours. It was sonicated for 4 hours, filtered, and then the filtrate obtained was dried using an oven at a temperature of 80 °C for 24 hours. The red algae $\text{NiCl}_2 \cdot 6\text{H}_2\text{O}$ powder was then ground and mixed with different proportions of 1 M KOH, with the ratio of red algae and 1 M KOH as follows: 1:0, 1:0.5, and 1:1. Each is marked with RA(Ni)0; RA(Ni)0.5 and RA(Ni)1, then transferred into a furnace tube. Samples were pyrolyzed at a temperature of 800 °C for 2 hours, so that a MAB composite was formed. During the mixing and pyrolysis stages, there is a possibility that $\text{NiCl}_2 \cdot 6\text{H}_2\text{O}$ reacts with KOH to form $\text{Ni}(\text{OH})_2$, which upon pyrolysis can transform into NiO. This NiO may be embedded within the carbon matrix and exist in nanoparticulate form. The presence of NiO nanoparticles is known to contribute to magnetic properties, especially exhibiting superparamagnetic behavior, which can enhance the functionality of the resulting composite. The MAB composite was cooled and rinsed with distilled water until the pH was neutral, followed by drying at 80 °C for 24 hours (Yao et al., 2020). KOH was used as a chemical activating agent to enhance the porous structure and surface area of the resulting biocarbon. During the high-temperature pyrolysis process, KOH chemically reacts with the carbon matrix, generating metallic potassium and potassium compounds such as K_2CO_3 . These products intercalate into the carbon lattice, creating micro- and mesopores through etching and expansion. This activation mechanism was expected to increase the availability of active sites and improve the overall adsorption capacity of the MAB composite.

The MAB composite samples of red algae that have been labelled RA(Ni)0; RA(Ni)0.5, RA(Ni)1, and RA(Ni)1.5, each were also tested for their maximum adsorption percentage (%E). Then, the four samples were compared with the %E relationship curve with each sample. %E was calculated using Equations 1 as follows. The formed MAB composites were characterized by scanning electron microscope (SEM), XRD, FTIR, PSA, and dye absorbance measurements using a UV-Vis spectrophotometer.

$$\%E = \frac{C_0 - C_e}{C_0} \times 100\% \quad (1)$$

where: %E – adsorption efficiency (%), C_0 – initial concentration of dyes (mg/L), C_e – final concentration of dyes (mg/L) [10].

Adsorption studies

Effect of pH

A total of 0.2 g of MAB composite mixed with 50 mL of MB (Cationic dye) solution (15 mg/L) in a 100 mL Erlenmeyer flask in various pH (1, 2, 3, 4, 5, 6, 7, 8, 9, 10, 11 and 12). The pH was adjusted by adding 0.1 M HCl or NaOH solution to conditioning pH towards acidic or basic solutions. The mixture was then stirred using a magnetic stirrer at 200 rpm for 60 minutes and filtered. The absorbance of the filtrate was measured using a UV-Vis spectrophotometer at maximum wavelength. The same procedure was conducted for the RBY dye (anionic dye).

Effect of contact time

A total of 0.2 g of MAB composite mixed with 50 mL of MB solution or RBY dye (15 mg/L) at optimum pH into a 100 mL Erlenmeyer flask. It was followed by stirring using a magnetic stirrer at 200 rpm for varying times and filtered. The absorbance of the filtrate was measured using a UV-Vis spectrophotometer at maximum wavelength. The following were done for various contact times of 20, 40, 60, 80, 100, and 120 minutes.

Effect of mass adsorbent

The MAB composites with various dosages (0.05 g, 0.1 g, 0.15 g, 0.2 g, 0.25 g, and 0.3 g.) and 50 mL of MB or RBY dye solution (15 mg/L) and optimum pH were mixed into a 100 mL Erlenmeyer flask. They were stirred using a magnetic stirrer for optimum contact time and then filtered. The absorbance of the filtrate was measured using a UV-Vis spectrophotometer at maximum wavelength. The following were done for activated carbon masses of 0.05 g, 0.1 g, 0.15 g, 0.2 g, 0.25 g, and 0.3 g.

Effect of dyes initial concentrations

A total of 50 mL of MB or RBY dyes solutions was added with varying concentrations (15, 20, 25, 30, and 35 mg/L) at optimum pH and

optimum dosages of MAB composite into a 100 mL Erlenmeyer flask. They were stirred with a magnetic stirrer at 200 rpm for optimum contact time, then filtered. The absorbance of the filtrate was measured using a UV-Vis spectrophotometer at maximum wavelength.

Regeneration

Firstly, 50 mL of MB or RBY dyes solution with optimum condition (concentration, pH, and MAB composite dosages) obtained from previous procedures was added into a 100 mL Erlenmeyer flask. The mixture was stirred with a magnetic stirrer at 200 rpm for optimum contact time, then filtered. The absorbance value was determined using a UV-Vis spectrophotometer at maximum wavelength. The MAB composite was rinsed with ethanol and repeated until the adsorbent was unable to absorb the dye.

Adsorption isotherm

The equilibrium amount of dye adsorption is calculated according to the absorbance value obtained and the concentration used, using Equation 2. The Freundlich isotherm can be determined by the Equations 3–4, while Langmuir isotherm can be determined by Equation 5.

$$Q_e = \frac{(C_0 - C_e)V}{m} \quad (2)$$

where: Q_e – equilibrium of the amount of dye adsorption, C_0 – initial concentration of dye (mg/L), C – equilibrium concentration of dye (mg/L), V – volume dye solution (L), m – weight of MAB composite (g).

$$\frac{x}{m} = K \cdot C_e^{1/n} \quad (3)$$

$$= \ln K + \frac{1}{n} \ln C \quad (4)$$

where: x/m – amount of adsorbed substance per unit mass of adsorbent (mg/g), C – equilibrium concentration of adsorbed substance in the liquid phase, K – Freundlich's constant relating to capacity, $1/n$ – Freundlich constant related to adsorption affinity.

$$x/m = \frac{qm \cdot C \cdot C_e}{1 + b \cdot C_e} \quad (5)$$

where: x/m – amount of adsorbed substance per unit mass of adsorbent (mg/g), Q_0 – constant related to adsorption capacity (mg/g), qm – adsorption capacity (mg/g), b – constant related to the adsorption rate (1/mg), C – equilibrium concentration of adsorbed substance in the liquid phase.

Characterization

The Shimadzu FTIR 8400, a Fourier transform infrared (FTIR) instrument with a range of 4000–400 cm^{-1} , was used to identify the functional

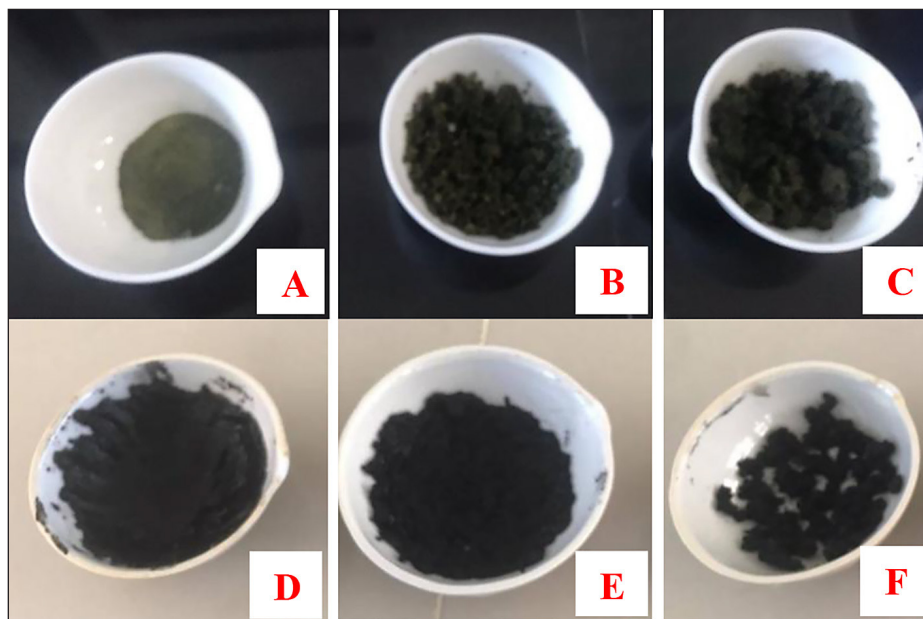


Figure 2. Visual photograph of: above – RA(Ni)0 (A), RA(Ni)0.5(B), and RA(Ni)1 (C) before pyrolysis; and below – RA(Ni)0 (D), RA(Ni)0.5 (E), and RA(Ni)1 (F) after pyrolysis

groups in the samples. Additionally, the XRD was used to identify the crystallinity of each sample, which was determined at $2\theta = 25 - 70^\circ$ using a $K\alpha$ (Cu) 1.54 as the source of the ray. A particle size analyzer (PSA) was used to measure the particle sizes of the samples. Lastly, scanning electron microscopy (SEM) was used to examine the surface morphology of the samples.

RESULTS AND DISCUSSION

Adsorption efficiency

The activation of magnetic red algae with varying concentrations of KOH enhances its adsorption capacity by increasing porosity and eliminating impurities. As a chemical activator, KOH facilitates the formation of a porous structure in the biocarbon derived from red algae, thereby improving its efficiency in adsorption and filtration applications. This activation process significantly enhances surface area and porosity, which are critical for optimizing adsorption performance (Harimisa et al., 2022; Tsarpali et al., 2024). Figure 2 presented the visual photograph of red algae magnetically using $NiCl_2 \cdot 6H_2O$ and different concentration of KOH before and after pyrolysis.

The optimal RA(Ni) composite was determined by evaluating its adsorption efficiency for MB and RBY removal. Adsorption experiments were conducted using a dye concentration of 15 mg/L at pH 7 for 60 minutes. The results indicated that the adsorption efficiencies of RA(Ni)0, RA(Ni)0.5, and RA(Ni)1 for MB removal were

89.18%, 91.6%, and 90.07%, respectively (Figure 3, blue lines). Meanwhile, the adsorption efficiencies for RBY removal were 61.36%, 71.30%, and 67.37%, respectively (Figure 3, yellow lines).

Figure 3 shows the addition of KOH improve the adsorption efficiency of the composite until 0.5 M. However, the increase in KOH concentration to 1 M reduces the adsorption efficiency. It was due to the high KOH concentration at high temperatures which damages the pore structure of red algae, thereby reducing adsorption performance. Studies have shown that excessive KOH used to activation of biocarbon, damaging its pore structure (Khamkeaw et al., 2023; Kierzek and Gryglewicz, 2020). The RA(Ni)0.5 composite shows the optimal adsorption performance, where its adsorption efficiency values for MB and RBY were 91.60% and 71.30%, respectively. Therefore, RA(Ni)0.5 was used for further studies.

Characterization

Fourier transform infrared (FTIR)

FTIR spectra of RA(Ni)0.5 before and after pyrolysis, and after adsorption MB and RBY are shown in Figure 4. The FTIR spectra of RA(Ni)0.5 before and after pyrolysis show the absorption bands of several functional groups, such as OH, NH, CO, CC, C=N, and Ni-O which are typical peaks of red algae and nickel.

The broad absorption band around 3400 cm^{-1} in spectrum A (RA(Ni)0.5) indicates the presence of hydroxyl (-OH) groups, which are characteristic of water molecules and oxygen-containing

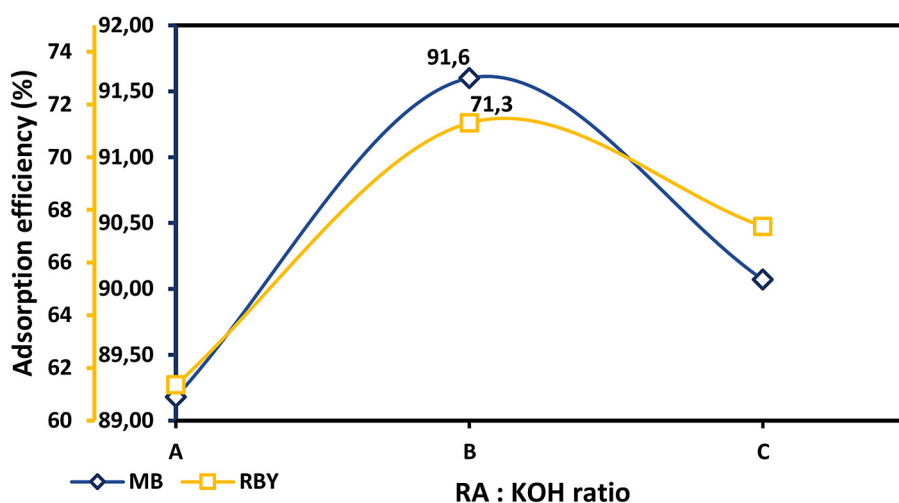


Figure 3. The adsorption efficiency of: RA(Ni)0 (A), RA(Ni)0.5 (B), and RA(Ni)1 (C) for MB (blue line) and RBY (yellow line) removal

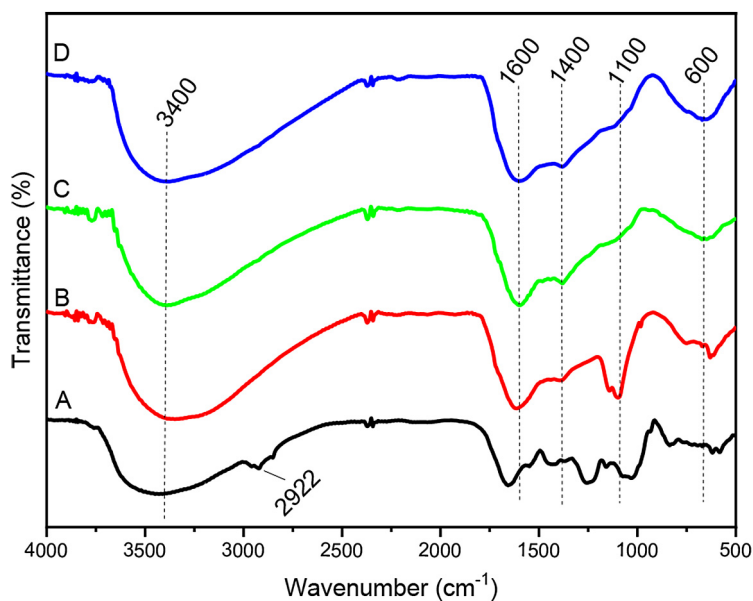


Figure 4. FTIR spectra of RA(Ni)0.5: before pyrolysis (A), after pyrolysis (B), after adsorption of MB and RBY, (C) and (D), respectively

functional groups in raw biomass (Jafarian et al., 2023; Tayibi et al., 2019). Similarly, the absorption band at 2922 cm^{-1} is attributed to the C-H stretching vibrations of aliphatic hydrocarbons. These findings align with previous studies that demonstrate how raw biomass typically contains hydroxyl-rich compounds from polysaccharide such as cellulose, hemicellulose, lignin, and protein (Călin et al., 2024; Matin & Aydin, 2022). The presence of these functional groups is critical in the initial structure of the red algae-based material, as they contribute to its hydrophilicity and potential interactions in adsorption applications. However, as pyrolysis progresses, these functional groups undergo significant transformations, leading to structural modifications in the material.

The FTIR spectrum of RA(Ni)0.5 after pyrolysis (spectrum B) shows a noticeable reduction in the intensity of the 3400 cm^{-1} band, suggesting the removal of hydroxyl groups due to thermal degradation. This observation is consistent with previous studies indicating that hydroxyl groups progressively disappear at higher pyrolysis temperatures (Călin et al., 2024; Zou et al., 2024). At temperatures above 500 °C , hydroxyl groups are largely eliminated, leading to the formation of a more carbonaceous and thermally stable material (Liu et al., 2015). Additionally, the significant reduction in the 2922 cm^{-1} peak implies the degradation of aliphatic compounds, aligning with the research showing that pyrolysis effectively removes volatile organic compounds, leaving

behind a more condensed carbon structure (Matin and Aydin, 2022).

The emergence of characteristic peaks at 1600 cm^{-1} , 1400 cm^{-1} , and 1100 cm^{-1} suggests the formation of aromatic C=C stretching vibrations (1600 cm^{-1}) and C-O stretching vibrations (1100 cm^{-1}). These spectral changes indicate the conversion of organic biomass into biochar, a process driven by the decomposition of polysaccharide at intermediate pyrolysis temperatures ($400\text{--}600\text{ °C}$) (Chen et al., 2019; He et al., 2021). The increase in aromaticity further supports the enhanced stability and adsorption capabilities of the material. The disappearance of hydroxyl (-OH) groups and aliphatic C-H vibrations is accompanied by the formation of new carbonaceous structures, including fused aromatic rings and oxygen-containing functional groups such as carboxyl and carbonyl species. This transformation is in agreement with the studies that describe how biomass undergoes carbonization, leading to the formation of a highly condensed structure at temperatures above 600 °C (Suman and Gautam, 2017; Zou et al., 2024). The structural changes observed in the FTIR spectrum confirm the biochar transition from a hydroxyl-rich precursor to a stable, porous material with enhanced adsorption potential. This transformation is crucial for applications in environmental remediation, particularly in adsorption-based technologies where surface chemistry plays a critical role (Hu et al., 2019; Menaa et al., 2021).

The FTIR spectra after adsorption of MB and RBY exhibit significant changes, particularly with the reappearance of the 3400 cm^{-1} band. This reappearance indicates the interaction of adsorbed dye molecules with hydroxyl ($-\text{OH}$) groups or water molecules. This observation aligns with the findings from Mokhtar et al. (2018) (Mokhtar et al., 2018) and Jiang et al. (2023) (Jiang et al., 2023), who reported that hydroxyl ($-\text{OH}$) and carbonyl ($\text{C}=\text{O}$) functional groups play a crucial role in dye adsorption by providing active binding sites. The hydroxyl groups, which were partially degraded during pyrolysis, seem to be involved in hydrogen bonding with the dye molecules, facilitating the adsorption process. The increased intensity of peaks at 1600 cm^{-1} and 1400 cm^{-1} suggests enhanced interactions between dye molecules and the functional groups on the $\text{RA}(\text{Ni})0.5$ surface. These peaks correspond to aromatic $\text{C}=\text{C}$ stretching and possible electrostatic interactions or hydrogen bonding between the dyes and the material.

The FTIR spectra before and after dye adsorption (Figure 4) show significant changes, particularly in the region around 1100 cm^{-1} . Prior to adsorption, a distinct peak was observed at $\sim 1100\text{ cm}^{-1}$, which corresponds to the $\text{C}-\text{O}$ stretching vibrations in alcohols, ethers, or possibly $\text{C}-\text{N}$ stretching in amines. However, this peak disappears after the adsorption of MB and RBY, particularly in spectra C and D. This disappearance suggests a strong involvement of $\text{C}-\text{O}$ or $\text{C}-\text{N}$ functional groups in the adsorption process. The binding of MB and RBY dye molecules likely occurs through electrostatic interactions and hydrogen bonding with these functional groups, leading to either the consumption or structural transformation of the groups responsible for the 1100 cm^{-1} band.

Jiang et al. (2023) reported that methylene blue adsorption on biochar is driven by $\pi-\pi$ interactions and electrostatic attractions between the cationic dye and oxygen-containing groups, such as hydroxyl and carbonyl (Jiang et al., 2023). The same applies to RBY, which interacts through hydrogen bonding and electrostatic attraction, particularly involving carbonyl and ether groups. Tang et al. (2024) also observed that the disappearance or broadening of specific FTIR peaks after adsorption indicates the active participation of the corresponding functional groups in dye binding (Tang et al., 2024). Therefore, the absence of the 1100 cm^{-1} peak supports the conclusion that these functional groups are actively involved in the dye adsorption process on the $\text{RA}(\text{Ni})0.5$ surface.

The presence of an adsorption band at 600 cm^{-1} , attributed to $\text{Ni}-\text{O}$ vibrations, indicates that metal-oxygen bonds contribute to the adsorption mechanism. The involvement of nickel sites in the composite structure may enhance adsorption by providing additional coordination sites for dye molecules. This finding aligns with previous studies demonstrating that nickel-based materials exhibit higher adsorption capacities due to strong $\text{Ni}-\text{O}$ interactions and enhanced surface functionalization (Bach et al., 2018; Yu and Tobilko, 2024). For example, the research by Zahara et al. (2023) reported that a $\text{Ni}-\text{Al}$ /magnetite biochar composite achieved an adsorption capacity of 68.493 mg/g , with $\text{Ni}-\text{O}$ bonds playing a crucial role in the adsorption process (Zahara et al., 2023). While the activation process enhances dye adsorption, it also results in the loss of some functional groups during pyrolysis. This trade-off between surface area enhancement and functional group preservation.

X-ray diffraction (XRD)

XRD characterization aims to determine the crystallinity of red algae. The results of XRD characterization of red algae before activation, after magnetic activation presented in Figure 5.

The intensity of the XRD diffraction peak of red algae (Figure 5) after activation ($\text{RA}(\text{Ni})0.5$) is higher than that of red algae before activation, this is due to the use of carbon in the KOH activation process and the increase in Ni metal content. The main Ni diffraction peak is centered between the 2θ angles of 40° and 80° . On the basis of the XRD results of $\text{RA}(\text{Ni})0.5$, the diffraction peaks are seen at the angles of $2\theta = 44.14^\circ$, 53.28° , and 62.16° , these results are in accordance with the nickel element (NiO) for $(1,1,1)$, $(2,0,0)$, $(2,2,0)$, which indicates that nickel metal has been successfully filled on the surface of $\text{BW}(\text{Ni})0.5$. Due to its strong magnetic properties, $\text{RA}(\text{Ni})0.5$ adsorbent can be easily separated from the adsorbate after the adsorption process. In addition, this $\text{RA}(\text{Ni})0.5$ adsorbent can be easily recycled for reuse as an adsorbent. The intensity of the XDR diffraction peak of $\text{BW}(\text{Ni})0.5$ after activation is seen to increase, which causes an increase in the crystallinity of the adsorbent. The formation of crystallinity in the MAB composite adsorbent, $\text{BW}(\text{Ni})0.5$ proves that the activation process using KOH causes Ni to be filled on the surface of the red algae biocarbon composite adsorbent.

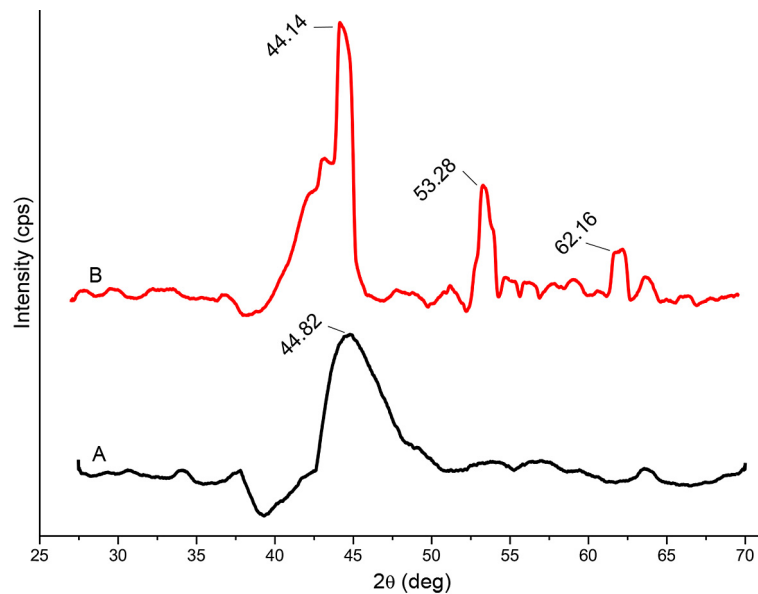


Figure 5. XRD diffractogram of red algae, before (A) and after (B), activation

Scanning electron microscope (SEM)

Characterization using SEM aims to determine the surface morphology of red algae. Surface morphology greatly affects the adsorption capacity of a sample. SEM characterization was carried out at 2.000x and 6.000x magnifications, as presented in Figure 6.

According to the SEM image in Figure 6, shown that the surface of RA(Ni) biocarbon composite without KOH treatment is irregular and lumpy, and no pore structure is visible (Figure 6A

and B). However, after being activated with KOH, the surface is more even, there are abundant pore structures on the surface of the RA(Ni)0.5 biocarbon composite (Figure 6C and D). This indicates that KOH plays an active role in the formation of biocarbon pores and the pore sizes are mainly mesopores and macropores (Musa et al., 2015). Also, as shown as the red arrow points in the SEM image of KOH-treated biocarbon, some point features on the surface of the MAB composite appear as nickel particles, and during high-temperature pyrolysis,

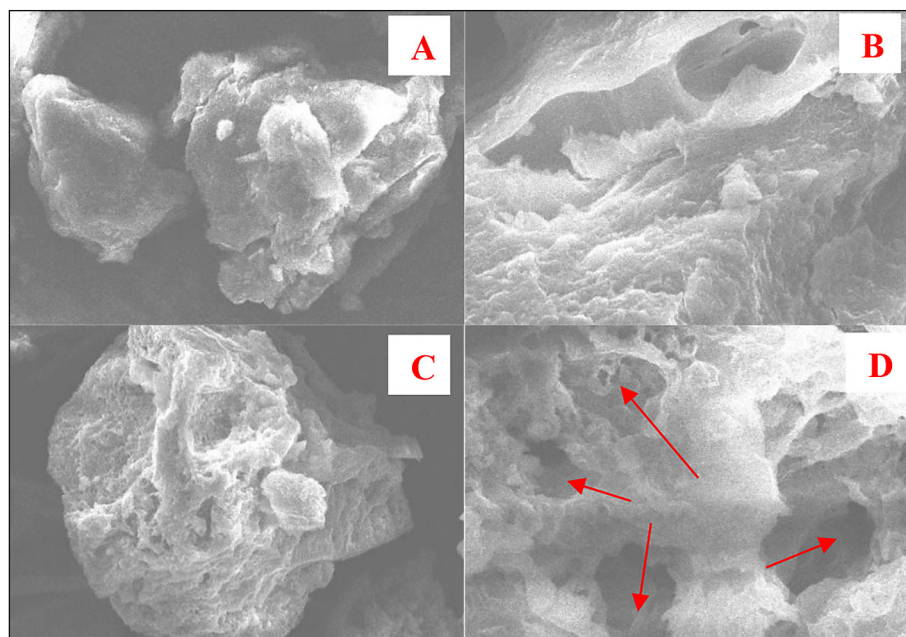


Figure 6. Red algae before activation (A and B) with 2000x and 6000x magnification, respectively; and after magnetic activation (C and D) with 2000x and 6000x magnification, respectively

nickel ions are reduced to nickel metal, which is embedded in the pores of biocarbon indicating the successful synthesis of biocarbon composite.

Particle size analyzer (PSA)

Particle size analyzer (PSA) aims to determine the particle size of MAB composites. Particle size greatly affects the adsorption capacity of a sample, due to large surface area of composites. The PSA profile of the present study is shown in Figure 7.

On the basis of the PSA result in Figure 7, it is known that the average particle size of the MAB composite obtained is 37.3 nm. The results of this study indicate that the MAB composite meets the nanoparticle size (< 100 nm) (nanocomposite). Smaller particle size increases the surface area and provides more active sites, thus enhancing dye adsorption. This nanostructure expected supports adsorption capacity of RA(Ni)0.5 for MB and RBY dyes. Furthermore, the nano-sized structure facilitates better contact between the dye molecules and the adsorbent surface, accelerating the adsorption kinetics and promoting more efficient pollutant removal.

Adsorption studies

Determination of optimum pH

Determination of optimum pH of adsorption aims to determine the optimum pH of dye that can be absorbed by the adsorbent. The pH value can affect the adsorption process of the ionic form of

the adsorbed dye, the nature of the adsorbate and the surface charge of the adsorbent used. Chemically, MB is cationic, where this dye will easily bind to the adsorbent at alkaline pH, while RBY is anionic, which makes it easier for the dye to bind to the adsorbent at acidic pH. The absorption efficiency (%E) of the RA(Ni)0.5 biocarbon composite for dyes both for the MB dye and the RBY dye tended to increase with increasing pH and the optimum pH for the MB and RBY dyes was obtained at pH 10 and 4, respectively. The relationship between pH variations and absorption efficiency (%E) is depicted in Figure 8.

Figure 8 shows the relationship between pH variation and adsorption efficiency (%E). Low pH values cause an increase in the concentration of H^+ ions in the system and the surface of activated carbon will be positively charged by absorbing H^+ ions. At a certain pH, cationic dyes can undergo protonation (accept H^+ ions) and turn into positive ions (cations), which can be more easily adsorbed by the negatively charged adsorbent surface. Conversely, at different pH, the ionization of cationic dyes can decrease, and this can reduce their affinity for the negatively charged surface of the adsorbent. This is due to the hydrophobic nature of biocarbon which causes it to absorb hydrogen ions (H^+) to the biocarbon surface. In general, the adsorption of cationic dyes tends to increase with decreasing pH (to acidic), because more cation ions are formed under these conditions, and increase the interaction with the negatively charged

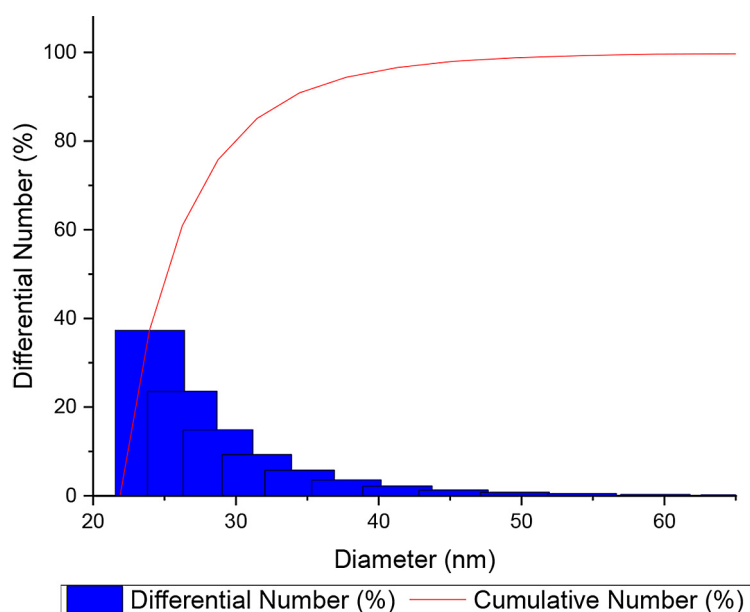


Figure 7. RA(Ni)0.5 particle size analysis

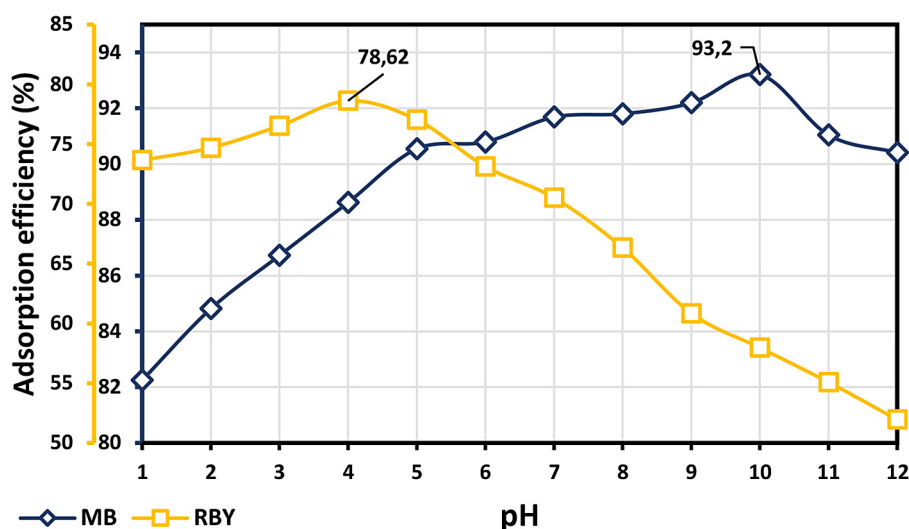


Figure 8. Effect of pH for MB (blue line) and RBY (yellow line) adsorption

surface of the adsorbent. However, at low pH, the surface of the adsorbent becomes too positively charged and can repel cationic ions from the dye, resulting in decreased adsorption capacity. The %E of this cationic dye (MB) tends to increase from pH 1–10 and tends to decrease at pH 11–12 so that the optimum pH is obtained at pH 10. This finding is slight different from previous reported study, where optimum pH for MB adsorption using magnetic biochar derived from *Ulva fasciata* marine algae (Kadimpati et al., 2024).

Anionic dyes can undergo deprotonation (loss of H^+ ions) and turn into negative ions (anions), which can be more easily adsorbed by the positively charged adsorbent surface. Conversely, at different pH, the ionization of anionic dyes can decrease, and this can reduce their affinity for the positively charged surface of the adsorbent. In general, the adsorption of anionic dyes tends to increase along with increasing pH, until it reaches the optimum pH. However, after the optimum pH, adsorption seems to start to decrease due to competition between H^+ ions (in the form of acid) and anions from the dye to interact with the adsorption sites on the adsorbent surface. The %E of this anionic dye (RBY) tends to increase from pH 1–4 and tends to decrease at pH 5–12 so that the optimum pH is obtained at pH 4. The decrease in pH in both dyes is because the adsorbent begins to saturate and causes many dyes that have not yet bound to the active sites of the adsorbent so that its adsorption power decreases. This finding is quite different from the previous study reported, where magnetite nanoparticles modified *Azolla* reach

optimum adsorption for RBY at pH 2 (Shariati et al., 2021). However, other finding reported that the optimum pH for RBY adsorption was 4 (Sukarta et al., 2025). Although the point of zero charge (pHpzc) of RA(Ni)0.5 was not measured directly in this study, the observed adsorption behavior suggests that the adsorbent surface carries a net positive charge below pH 4 and a net negative charge above pH 10. This highlights the role of surface charge in the adsorption mechanism. Future studies should include a pHpzc analysis to provide a clearer understanding of the surface charge behavior of the composite

Determination of optimum contact time

Determination of optimum adsorption contact time aims to determine the optimum time for dyes that can be absorbed by the adsorbent. However, when the adsorbent cannot absorb the dye, the adsorbent has reached saturation point. Determination of optimum contact time is determined at a dye concentration of 15 mg/L, pH 10 and 4 for MB and RBY, respectively. The results show that the optimum contact time for dye adsorption using MAB composites is obtained at 80 minutes for MB with %E of 93.46% and 60 minutes for RBY with %E of 86.46%. The relationship between adsorption time variation and absorption efficiency (%E) is presented in Figure 9.

On the basis of Figure 9, it was shown the relationship between contact time variation with absorption efficiency (%E), in MB adsorption. The absorption efficiency (%E) tends to increase at contact time at first of 20–80 minutes,

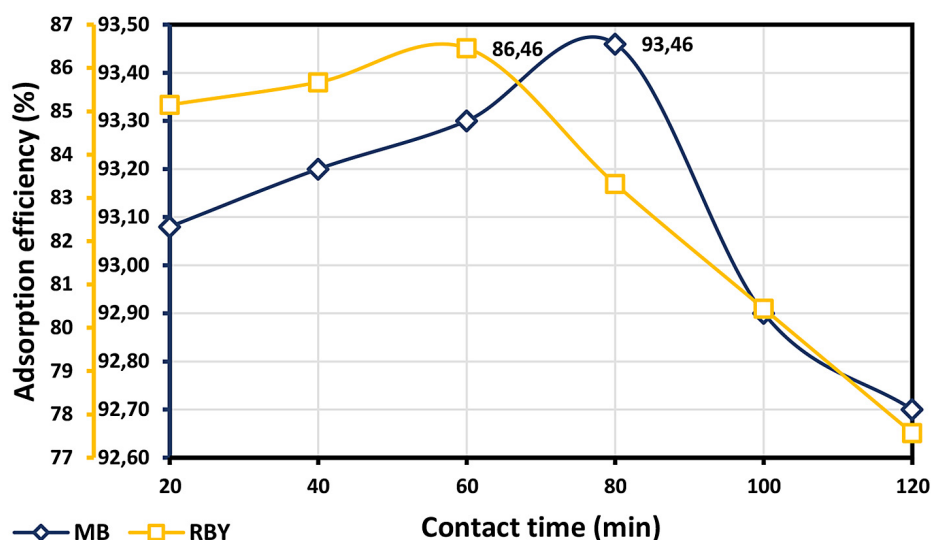


Figure 9. Effect of contact time for MB (blue line) and RBY (yellow line) adsorption

and tends to decrease at contact time of 100–120 minutes. The contact time in this study aligning with previous studies on MB adsorption, contact time increase in first one hour, and continued decrease after contact time increased (Kadimpati et al., 2024; Shi et al., 2022). While in RBY adsorption, absorption efficiency (%E) tends to increase at time of 20–60 minutes and tends to decrease at 80–120 minutes. This finding is quite different from the other study, with optimum contact time for MB removal using biochar from coffee fruit shell waste at 80 minute (Sukarta et al., 2025). The presented study reported the fastest contact time for removal RBY using biocarbon based adsorbent, compared to the previous study.

Determination of optimum adsorbent dosages

The determination of the optimum adsorbent mass for adsorption aims to determine the optimum adsorbent mass that can absorb dyes. The determination of the optimum adsorption mass is then determined at a dye concentration of 15 mg/L, pH 10, 80 minutes for MB and at a dye concentration of 15 mg/L, pH 4, 60 minutes for RBY. The optimum mass of the MAB composite adsorbent is 0.1 and 0.2 g for MB (%E of 93.46%) and RBY (%E of 88.02%), respectively. The relationship between mass variation and absorption efficiency (%E) is presented in Figure 10. The effect of dosage on adsorption capacity of MB and

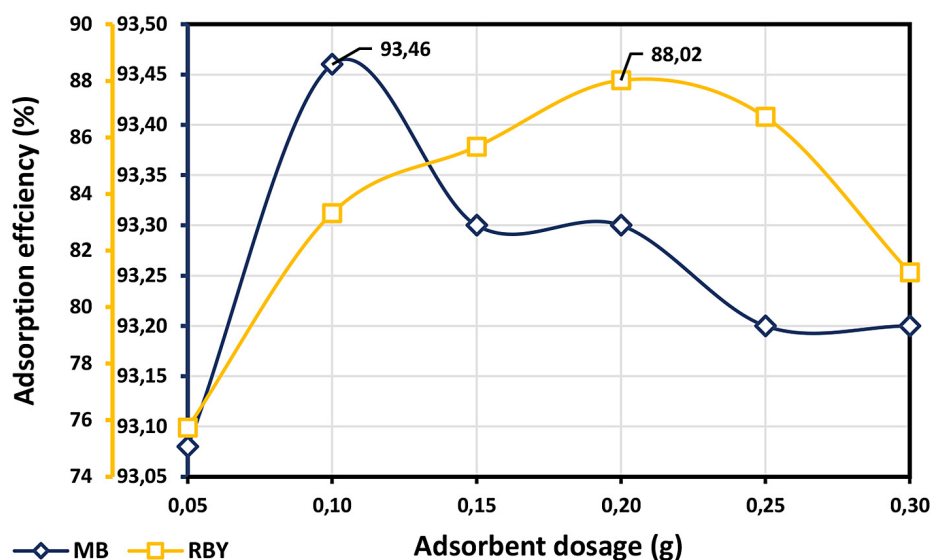


Figure 10. Optimum adsorbent dosage for MB (blue line) and RBY (yellow line) adsorption

RBV dyes as presented in Figure 10 shows the relationship between the variation of adsorbent mass and %E. The results generally show that the increasing the dosage of adsorbent used (0.05 to 0.1 g for MB and 0.05 to 0.2 g), the more effective the adsorption process occurs. However, the adsorption efficiency was decrease after increasing the dosage of adsorbent from 0.1 to 0.3 g in MB dye removal. In other hand, the adsorption efficiency of the adsorbent to RBV dye tends to decrease at dosage more than 0.25 g. In general, dye absorption increases with increasing adsorbent mass, this is due to the increasing surface area and there are more active adsorption sites that can absorb dyes completely (Hashem et al., 2024). While when reaching the optimum adsorbent mass, the adsorption power decreases. This is due to the adsorbent begins to saturate, causes many dyes that have not bonded to the active sites of the adsorbent so that its efficiency is getting smaller (Alotaibi et al., 2024; Bayat et al., 2023; Foroutan et al., 2021). Other study also reported that, this possibly due to adsorbent particle was collide and the adsorption efficiency significantly decreased (Hashem et al., 2024).

Effect of dyes initial concentration

Determination initial concentration aims to determine the optimum concentration of dye that can be absorbed by the adsorbent. Determination of optimum of initial concentration was carried out at pH 10, adsorbent dosage 0.1 g for 80 minutes, and pH 4, adsorbent dosage 0.2 g, for 60

minutes, for MB and RBV dye, with various of dye concentration of 15, 20, 25, 30, and 35 mg/L. The results presented in Figure 11, the finding showed that the optimum initial concentration of both dyes occurred at 35 mg/L with %E 95.99 and 89.94% for MB and RBV, respectively.

On the basis of Figure 11, the linear relationship between the variation of dye concentration with %E was shown. The absorption efficiency increases along with the initial concentration of the dye. This finding is quite different from other reported, increasing the initial concentration cause decreased the adsorption efficiency, due to saturated of adsorbent active site at excess dyes concentration and increased the repulsive electrostatic force between dye and surface of adsorbent in aqueous solutions (Foroutan et al., 2021). This is possible because the adsorbent has not reached a saturated condition, so that it can still absorb dye molecules.

Adsorption isotherms studies

The adsorption process of RA(Ni)0.5 in removing dyes from water is influenced by many factors and has a specific isotherm pattern. The factors influencing the adsorption process include the type of adsorbent, pH, surface area, contact time and dosage of the adsorbent, and the type and initial concentration of adsorbate. Due to these factors, the adsorbents that absorb from one substance to another do not show the same adsorption isotherm pattern. However, the Langmuir

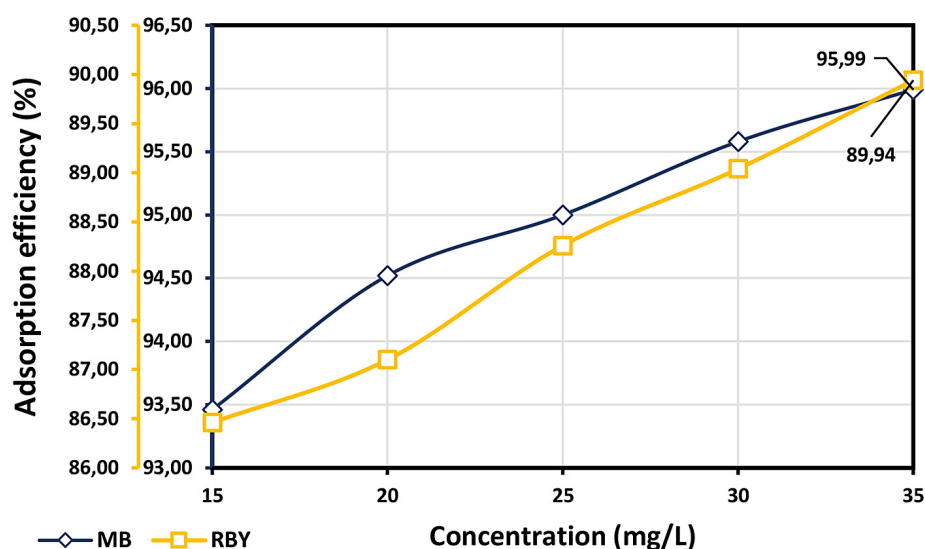


Figure 11. Determination of optimum initial concentration for MB (blue line) and RBV (yellow line) adsorption

and Freundlich adsorption equations, two types of adsorption isotherm equations, play a crucial role in understanding and predicting these patterns. These equations, which are commonly used in the solution absorption process, provide a solid foundation for studying the adsorption mechanism. Solid-liquid adsorption generally follows the Freundlich and Langmuir isotherm types. The adsorbate molecules and the adsorbate surface can bind by chemisorption-physisorption.

Freundlich Isotherm

The Freundlich isotherm equation on the adsorption of MB and RBY dyes was $y = 2.3646x + 0.8687$ (R^2 of 0.9914) (Figure 12A), and $y = 1.5986x + 0.003$ (R^2 of 0.9871), respectively (Figure 12B). The values of K_f are the Freundlich constant and n is a surface heterogeneity measure in this study, are calculated using these equations. There is a clear correlation between K_f and adsorption capacity. Stronger adsorption at low concentrations is indicated by a value of $n > 1$, which suggests that adsorption dramatically rises as the substance's concentration in the fluid phase decreases. Stronger adsorption at high concentrations is indicated by a value of $n < 1$, which means that adsorption diminishes as the fluid phase substance concentration falls. A value of $n = 1$ indicates linear adsorption to the fluid phase concentration of the chemical. These findings have practical applications in understanding and predicting adsorption behavior, particularly in environmental science and chemistry. The Freundlich isotherm model, included in the physical isotherm, describes adsorption on the surface of a solid, assuming that adsorption occurs on a heterogeneous solid surface, where adsorption does not occur at only one type of adsorption site.

Langmuir isotherm

The Langmuir isotherm of the present study obtained equation $y = 0.2628x + 0.1286$ (R^2 of 0.9892) and $y = 0.8685x + 0.115$ (R^2 of 0.995) for MB (Figure 13B) and RBY (Figure 13A) adsorption, respectively. These equations are used to determine the values of Q_m and K_l , where Q_m represents the maximum adsorption capacity under ideal conditions, assuming that each adsorption site can only accommodate a single molecule. Meanwhile, K_l is the Langmuir constant, which describes the bond strength or affinity between the adsorbate and the solid surface. The b value indicates the degree of adsorption as the adsorbate concentration in the fluid phase increases. The Langmuir isotherm model is based on chemical assumptions and describes the interaction between adsorbed molecules and the solid surface. This model assumes that adsorption occurs on a homogeneous surface, with each adsorption site capable of binding only one molecule. It relies on the concept of chemical equilibrium between molecules in the fluid phase and those adsorbed on the solid surface.

To determine the most suitable isotherm model for this study, refer to Table 1. The selection of the isotherm model is based on the correlation coefficient (R^2) value. According to the data presented in the table, for MB dye adsorption, the R^2 value for the Freundlich isotherm is 0.9914, while for the Langmuir isotherm, it is 0.9892. In contrast, for RBY dye adsorption, the R^2 value for the Freundlich isotherm is 0.9871, whereas for the Langmuir isotherm, it is 0.995. On the basis of these findings, the adsorption of MB follows the Freundlich isotherm model, while the adsorption of RBY is best described by the Langmuir isotherm model. This conclusion is supported by the

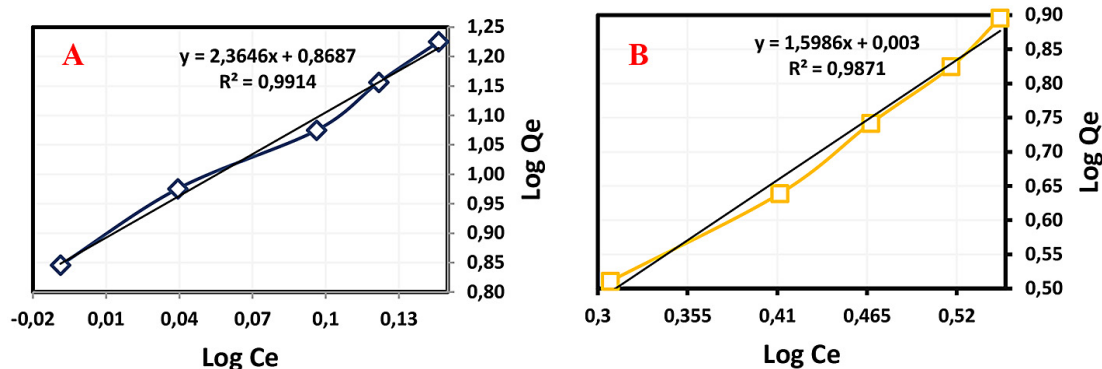


Figure 12. Freundlich isotherm equation for MB (A) and RBY (B) dyes

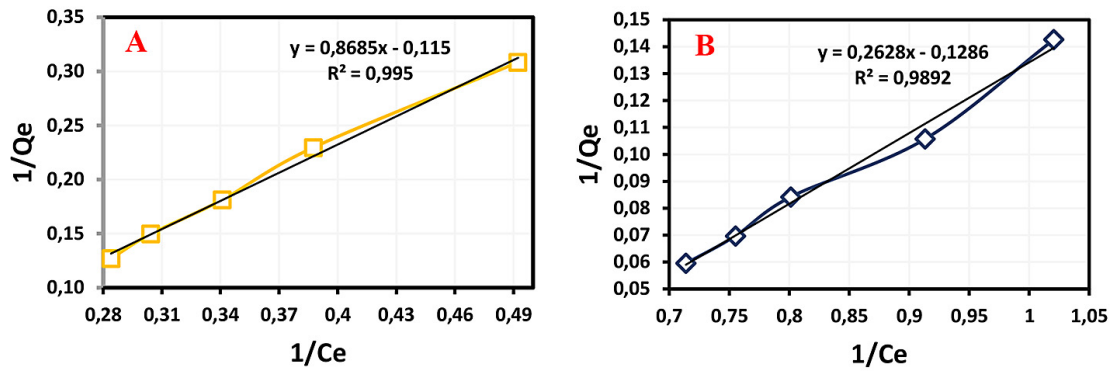


Figure 13. Langmuir isotherm equation RBY (A) and MB (B) dyes

Table 1. Determination of adsorption isotherm

Dyes	Freundlich isotherm			Langmuir Isotherm		
	Kf (mg/g)	n	R ²	Qm (mg/g)	Kl	R ²
MB	7.3909	0.4229	0.9914	0.7882	4.8285	0.9892
RBY	1.0069	0.6255	0.9871	8,6956	0.1324	0.9950

correlation coefficient (R^2) values, which indicate the best-fitting model for each adsorption process.

Regeneration

The surface of the algal biocarbon loaded with nickel is easily separated from the water phase by external magnetic force. It has a higher recovery rate, which is good and convenient for reuse. As the research has been done, the adsorbent changes the blue color (MB) and yellow color (RBY) into a turbid black solution. For 15 times of adsorption and desorption recycling, the percentage of

adsorption of MAB composite adsorbent to MB dye was 95.83, 95.61, 95.18, 94.90, 94.58, 94.30, 92.94, 92.18, 90.32, 89.40, 87.54, 86.70, 85.53, 84.22, and 83.02%, respectively, while the RBY dye was 89.82, 89.26, 88.93, 88.48, 87.70, 87.33, 85.23, 82.54, 81.64, 79.63, 77.72, 75.37, 73.02, 70.22, and 67.08%.

The recycling results in Figure 14 showed that the MAB composite-based adsorbent has superior capacity remove dyes (MB and RBY), even though it has been used up to 15 times. The adsorption efficiency of MB and RBY using MAB composites-based adsorbent decreased in

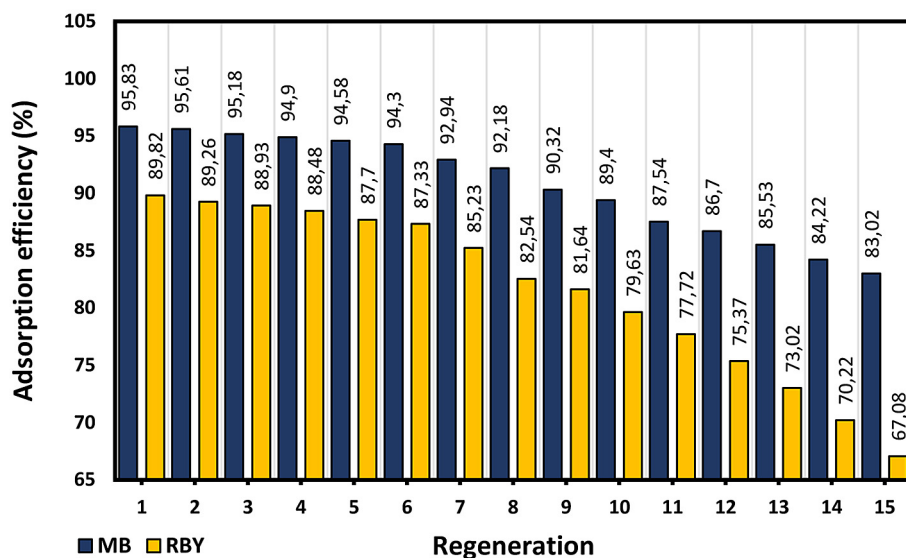


Figure 14. Regenerations of composite on MB (blue) and RBY (yellow) adsorption

low percentage by 13.37% and 24.87%, respectively, after 15 regeneration cycles. The recycling results also show that the adsorption capacity of the MAB composite adsorbent for both dyes decreases with an increasing number of cycles, which may be caused by the unavailability of some active sites after the reaction of functional groups with the composite. Another reason may be that some mesopores or micropores are filled and not completely washed during decomposition. On the basis of the overall recycling results, which are 15 repetitions, it shows that the MAB composite adsorbent is still good for use as a dye adsorbent for both MB and RBY dyes.

CONCLUSIONS

The MAB composite was successfully obtained under optimum removal conditions 91.60 and 71.30% for MB and RBY, respectively. FTIR analysis confirmed the presence of functional groups such as OH, NH, CO, C=C, C=N, and Ni–O, which are associated with red algae, the dyes, and nickel components. XRD results showed that the intensity of RA(Ni)0.5 increased compared to before activation, indicating successful incorporation of nickel and improved crystallinity. SEM images revealed that RA(Ni)0.5 had a more uniform surface and abundant pore structure compared to RA(Ni). PSA analysis confirmed that the average particle size of the RA(Ni)0.5 composite was 37.3 nm, indicating nanoscale dimensions. The optimum adsorption condition for MB was at pH 10, 80 minutes contact time, 0.1 g adsorbent mass, and 35 mg/L dye concentration, resulting in an adsorption capacity of 16.799 mg/g. For RBY, the optimum condition was at pH 4, 60 minutes, 0.2 g adsorbent, and 35 mg/L dye concentration, with an adsorption capacity of 7.869 mg/g. The MAB composite also showed excellent regeneration ability over 15 adsorption–desorption cycles for both dyes. These results highlight the great potential of red algae-based MAB composites as efficient and sustainable adsorbents for removing dyes from textile industry wastewater.

REFERENCES

1. Abdel-Aziz, A. B., Mohamed, N., El-taweel, R. M., Husien, S., Hung, Y.-T., Said, L. A., Fahim, I. S., Radwan, A. G. (2024). Crystal violet removal using

- algae-based activated carbon and its composites with bimetallic Fe 0–Cu. *Materials Research Express*, 11(6), 065801. <https://doi.org/10.1088/2053-1591/ad4e9c>
2. Abou Oualid, H., Abdellaoui, Y., Laabd, M., El Ouardi, M., Brahmi, Y., Iazza, M., Abou Oualid, J. (2020). Eco-efficient green seaweed codium decorticatum biosorbent for textile dyes: Characterization, mechanism, recyclability, and RSM optimization. *ACS Omega*, 5(35), 22192–22207. <https://doi.org/10.1021/acsomega.0c02311>
3. Al-Tohamy, R., Ali, S. S., Li, F., Okasha, K. M., Mahmoud, Y. A. G., Elsamahy, T., Jiao, H., Fu, Y., Sun, J. (2022). A critical review on the treatment of dye-containing wastewater: Ecotoxicological and health concerns of textile dyes and possible remediation approaches for environmental safety. *Ecotoxicology and Environmental Safety*, 231, 113160. <https://doi.org/10.1016/j.ecoenv.2021.113160>
4. Algarni, T. saad, Al-Mohaimeed, A. M. (2022). Water purification by adsorption of pigments or pollutants via metaloxide. *Journal of King Saud University - Science*, 34(8), 102339. <https://doi.org/10.1016/j.jksus.2022.102339>
5. Alotaibi, A. M., Alnawmasi, J. S., Alshammari, N. A. H., Abomuti, M. A., Elsayed, N. H., El-Desouky, M. G. (2024). Industrial dye absorption and elimination from aqueous solutions through bio-composite construction of an organic framework encased in food-grade algae and alginate: Adsorption isotherm, kinetics, thermodynamics, and optimization by Box–Behnken design. *International Journal of Biological Macromolecules*, 274, 133442. <https://doi.org/10.1016/j.ijbiomac.2024.133442>
6. Bach, L. G., Van Tran, T., Nguyen, T. D., Van Pham, T., Do, S. T. (2018). Enhanced adsorption of methylene blue onto graphene oxide-doped XFe₂O₄ (X = Co, Mn, Ni) nanocomposites: kinetic, isothermal, thermodynamic and recyclability studies. *Research on Chemical Intermediates*, 44(3), 1661–1687. <https://doi.org/10.1007/s11164-017-3191-1>
7. Bayat, M., Salehi, E., Mahdieh, M. (2023). Chromochloris zofingiensis microalgae as a potential dye adsorbent: Adsorption thermo-kinetic, isothermal, and process optimization. *Algal Research*, 71, 103043. <https://doi.org/10.1016/j.algal.2023.103043>
8. Boukarma, L., Aziam, R., Aboussabek, A., El Qdhy, S., Zerbet, M., Sinan, F., Chiban, M. (2024). Novel insights into crystal violet dye adsorption onto various macroalgae: Comparative study, recyclability and overview of chromium (VI) removal. *Bioresource Technology*, 394, 130197. <https://doi.org/10.1016/j.biortech.2023.130197>
9. Buhani, Wijayanti, T. A., Suharso, Sumadi, Ansori, M. (2021). Application of modified green algae Nanochloropsis sp. as adsorbent in the simultaneous

- adsorption of Methylene Blue and Cu(II) cations in solution. *Sustainable Environment Research*, 31(1), 17. <https://doi.org/10.1186/s42834-021-00090-y>
10. Călin, C., Sirbu, E.-E., Tănase, M., György, R., Popovici, D. R., Banu, I. (2024). A thermogravimetric analysis of biomass conversion to biochar: experimental and kinetic modeling. *Applied Sciences*, 14(21), 9856. <https://doi.org/10.3390/app14219856>
 11. Chen, Y., Liu, B., Yang, H., Wang, X., Zhang, X., Chen, H. (2019). Generalized two-dimensional correlation infrared spectroscopy to reveal the mechanisms of lignocellulosic biomass pyrolysis. *Proceedings of the Combustion Institute*, 37(3), 3013–3021. <https://doi.org/10.1016/j.proci.2018.06.141>
 12. Fakhri, V., Jafari, A., Layaei Vahed, F., Su, C.-H., Pirouzfard, V. (2023). Polysaccharides as eco-friendly bio-adsorbents for wastewater remediation: Current state and future perspective. *Journal of Water Process Engineering*, 54, 103980. <https://doi.org/10.1016/j.jwpe.2023.103980>
 13. Fathana, H., Adlim, M., Lubis, S., Iqhrammullah, M., Rahmi. (2023a). Chitosan film composite with sugarcane bagasse-derived cellulose filler for methylene blue adsorptive removal. *RASAYAN Journal of Chemistry*, 16(02), 543–548. <https://doi.org/10.31788/RJC.2023.1628204>
 14. Fathana, H., Rahmi, Adlim, M., Lubis, S. (2023b). Modification of chitosan using glycidyl methacrylate-grafted cellulose (GMAgCell/ Chi) for methylene blue adsorption. *Karbala International Journal of Modern Science*, 9(4), 687–697. <https://doi.org/10.33640/2405-609X.3322>
 15. Fathana, H., Rahmi, Adlim, M., Lubis, S., Iqhrammullah, M. (2023c). Sugarcane bagasse-derived cellulose as an eco-friendly adsorbent for azo dye removal. *International Journal of Design & Nature and Ecodynamics*, 18(1), 11–20. <https://doi.org/10.18280/ij dne.180102>
 16. Fazal, T., Faisal, A., Mushtaq, A., Hafeez, A., Javed, F., Alaud Din, A., Rashid, N., Aslam, M., Rehman, M. S. U., Rehman, F. (2021). Macroalgae and coal-based biochar as a sustainable bioresource reuse for treatment of textile wastewater. *Biomass Conversion and Biorefinery*, 11(5), 1491–1506. <https://doi.org/10.1007/s13399-019-00555-6>
 17. Foroutan, R., Peighambar-doust, S. J., Peighambar-doust, S. H., Pateiro, M., Lorenzo, J. M. (2021). Adsorption of crystal violet dye using activated carbon of lemon wood and activated Carbon/Fe₃O₄ magnetic nanocomposite from aqueous solutions: a kinetic, equilibrium and thermodynamic study. *Molecules*, 26(8), 2241. <https://doi.org/10.3390/molecules26082241>
 18. Harimisa, G. E., Jusoh, N. W. C., Tan, L. S., Shamel, K., Ghafar, N. A., Masudi, A. (2022). Synthesis of potassium hydroxide-treated activated carbon via one-step activation method. *Journal of Physics: Conference Series*, 2259(1), 012009. <https://doi.org/10.1088/1742-6596/2259/1/012009>
 19. Hashem, A., Aniagor, C. O., Farag, S., Fikry, M., Aly, A. A., Amr, A. (2024). Evaluation of the adsorption capacity of surfactant-modified biomass in an aqueous acid blue 193 system. *Waste Management Bulletin*, 2(1), 172–183. <https://doi.org/10.1016/j.wmb.2024.01.004>
 20. He, Z., Guo, M., Fortier, C., Cao, X., Schmidt-Rohr, K. (2021). Fourier transform infrared and solid state ¹³C nuclear magnetic resonance spectroscopic characterization of defatted cottonseed meal-based biochars. *Modern Applied Science*, 15(1), 108. <https://doi.org/10.5539/mas.v15n1p108>
 21. Hemavathy, R. V., Ragini, Y. P., Shruthi, S., Ranjani, S., Subhashini, S., Thamarai, P. (2025). Biofuel production from marine macroalgae: Pathways, technologies, and sustainable energy solutions. *Industrial Crops and Products*, 224(December 2024), 120282. <https://doi.org/10.1016/j.indcrop.2024.120282>
 22. Hu, E., Shang, S., Wang, N., Nan, X., Zhong, S., Yuan, Z. (2019). Influence of the pyrolytic temperature and feedstock on the characteristics and naphthalene adsorption of crop straw-derived biochars. *BioResources*, 14(2), 2885–2902. <https://doi.org/10.15376/biores.14.2.2885-2902>
 23. Jafarian, S., Bolouk, A. M. L., Norouzian, R., Taghavi, S., Mousavi, F., Kianpour, E., Signoretto, M. (2023). Sargassum macro-algae-derived activated bio-char as a sustainable and cost-effective adsorbent for cationic dyes: A joint experimental and DFT study. *Colloids and Surfaces A: Physicochemical and Engineering Aspects*, 678(September), 132397. <https://doi.org/10.1016/j.colsurfa.2023.132397>
 24. Jiang, D., Li, H., Cheng, X., Ling, Q., Chen, H., Barati, B., Yao, Q., Abomohra, A., Hu, X., Bartocci, P., & Wang, S. (2023). A mechanism study of methylene blue adsorption on seaweed biomass derived carbon: From macroscopic to microscopic scale. *Process Safety and Environmental Protection*, 172(November 2022), 1132–1143. <https://doi.org/10.1016/j.psep.2023.02.044>
 25. Julinawati, J., Febriani, F., Mustafa, I., Fathurahmi, F., Rahmi, R., Sheilatina, S., Ahmad, K., Puspita, K., Iqhrammullah, M. (2023). Tryptophan-based organoclay for aqueous naphthol blue black removal – preparation, characterization, and batch adsorption studies. *Journal of Ecological Engineering*, 24(7), 274–284. <https://doi.org/10.12911/22998993/165781>
 26. Kacaribu, A. A., Darwin, D. (2024). Biotechnological lactic acid production from low-cost renewable sources via anaerobic microbial processes. *BioTechnology*, 105(2), 179–194. <https://doi.org/10.5114/bta.2024.139757>

27. Kadimpati, K. K., Gnida, A., Turek-Szytow, J., Hellal, M. S., Gregor, M., Matula, G., Pawlyta, M., Monfort, O. (2024). Design of innovative hybrid biochar prepared from marine algae and magnetite: Insights into adsorption performance and mechanism. *Chemical Engineering Research and Design*, 201, 218–227. <https://doi.org/https://doi.org/10.1016/j.cherd.2023.11.053>
28. Khamkeaw, A., Sanprom, W., Phisalaphong, M. (2023). Activated carbon from bacterial cellulose by potassium hydroxide activation as an effective adsorbent for removal of ammonium ion from aqueous solution. *Case Studies in Chemical and Environmental Engineering*, 8(September), 100499. <https://doi.org/10.1016/j.cscee.2023.100499>
29. Khan, A. A., Naqvi, S. R., Ali, I., Arshad, M., Al-Mohamadi, H., Sikandar, U. (2023). Algal-derived biochar as an efficient adsorbent for removal of Cr (VI) in textile industry wastewater: Non-linear isotherm, kinetics and ANN studies. *Chemosphere*, 316, 137826. <https://doi.org/10.1016/j.chemosphere.2023.137826>
30. Kierzek, K., Gryglewicz, G. (2020). Activated carbons and their evaluation in electric double layer capacitors. *Molecules*, 25(18), 4255. <https://doi.org/10.3390/molecules25184255>
31. Lellis, B., Fávaro-Polonio, C. Z., Pamphile, J. A., Polonio, J. C. (2019). Effects of textile dyes on health and the environment and bioremediation potential of living organisms. *Biotechnology Research and Innovation*, 3(2), 275–290. <https://doi.org/10.1016/j.biori.2019.09.001>
32. Liu, Y., He, Z., Uchimiya, M. (2015). Comparison of biochar formation from various agricultural by-products using FTIR spectroscopy. *Modern Applied Science*, 9(4), 246–253. <https://doi.org/10.5539/mas.v9n4p246>
33. Matin, N. H., Aydin, E. (2022). Reviewing the effect of pyrolysis temperature on the fourier-transform infrared spectra of biochars. *Acta Horticulturae et Regiotecturae*, 25(2), 160–173. <https://doi.org/10.2478/ahr-2022-0020>
34. Menaa, F., Wijesinghe, U., Thiripuranathar, G., Althobaiti, N. A., Albalawi, A. E., Khan, B. A., & Menaa, B. (2021). Marine algae-derived bioactive compounds: A new wave of nanodrugs? *Marine Drugs*, 19(9), 484. <https://doi.org/10.3390/md19090484>
35. Mokhtar, N., A.Aziz, E., Aris, A., W.Ishak, W. F., Abdul Halim, H., Johari, N., N.Moni, S. (2018). Removal of methylene blue by red macro alga *Eucheuma Spinosum* Sp.: Pretreatment and desorption assessment. *International Journal of Engineering & Technology*, 7(4.35), 578–582. <https://doi.org/10.14419/ijet.v7i4.35.22916>
36. Musa, M. S., Sanagi, M. M., Nur, H., Wan Ibrahim, W. A. (2015). Understanding pore formation and structural deformation in carbon spheres during KOH activation. *Sains Malaysiana*, 44(4), 613–618. <https://doi.org/10.17576/jsm-2015-4404-17>
37. Periyasamy, A. P. (2024). Recent advances in the remediation of textile-dye-containing wastewater: prioritizing human health and sustainable wastewater treatment. *Sustainability (Switzerland)*, 16(2). <https://doi.org/10.3390/su16020495>
38. Prisa, D., Fresco, R., Jamal, A., Saeed, M. F., Spagnuolo, D. (2024). Exploring the Potential of macroalgae for sustainable crop production in agriculture. *Life*, 14(10), 1263. <https://doi.org/10.3390/life14101263>
39. Rahmi. (2018). Preparation of chitosan composite film using activated carbon from oil palm empty fruit bunch for Cd²⁺ removal from water. *IOP Conference Series: Materials Science and Engineering*, 434(1), 012071. <https://doi.org/10.1088/1757-899X/434/1/012071>
40. Rahmi, L., Julinawati, S. (2017). Preparation of chitosan composite film reinforced with cellulose isolated from oil palm empty fruit bunch and application in cadmium ions removal from aqueous solutions. *Carbohydrate Polymers*, 170, 226–233. <https://doi.org/10.1016/j.carbpol.2017.04.084>
41. Rahmi, L., Nurfatimah, R. (2018). Preparation of polyethylene glycol diglycidyl ether (PEDGE) cross-linked chitosan/activated carbon composite film for Cd²⁺ removal. *Carbohydrate Polymers*, 199, 499–505. <https://doi.org/10.1016/j.carbpol.2018.07.051>
42. Rahmi, Lubis, S., Az-Zahra, N., Puspita, K., Iqhrammullah, M. (2021). Synergetic photocatalytic and adsorptive removals of metanil yellow using TiO₂/grass-derived cellulose/chitosan (TiO₂/GC/CH) film composite. *International Journal of Engineering*, 34(8), 1827–1836. <https://doi.org/10.5829/ije.2021.34.08b.03>
43. Rahmi, R., Lelifajri, L., Iqbal, M., Fathurrahmi, F., Jalaluddin, J., Sembiring, R., Farida, M., Iqhrammullah, M. (2023). Preparation, characterization and adsorption study of PEDGE-cross-linked magnetic chitosan (PEDGE-MCh) microspheres for Cd²⁺ removal. *Arabian Journal for Science and Engineering*, 48(1), 159–167. <https://doi.org/10.1007/s13369-022-06786-6>
44. Shariati, F., Shariati, S., Moghaddam, M. A. A. (2021). Application of magnetite nanoparticles modified Azolla as an adsorbent for removal of reactive yellow dye from aqueous solutions. *Desalination and Water Treatment*, 212, 323–332. <https://doi.org/10.5004/dwt.2021.26612>
45. Shi, Y., Wang, H., Song, G., Zhang, Y., Tong, L., Sun, Y., Ding, G. (2022). Magnetic graphene oxide for methylene blue removal: adsorption performance and comparison of regeneration methods.

- Environmental Science and Pollution Research*, 29(20), 30774–30789. <https://doi.org/10.1007/s11356-021-17654-5>
46. Show, S., Akhter, R., Paul, I., Das, P., Bal, M., Bhattacharya, R., Bose, D., Mondal, A., Saha, S., Halder, G. (2024). Efficacy of exopolysaccharide in dye-laden wastewater treatment: A comprehensive review. *Chemosphere*, 355, 141753. <https://doi.org/10.1016/j.chemosphere.2024.141753>
 47. Sukarta, I. N., Suyasa, I. W. B., Mahardika, I. G., Suprihatin, I. E., Sastrawidana, I. D. K. (2025). Innovation of remazol yellow FG dye adsorption using biochar from coffee fruit shell waste. *Journal of Ecological Engineering*, 26(1), 273–285. <https://doi.org/10.12911/22998993/195754>
 48. Suman, S., Gautam, S. (2017). Pyrolysis of coconut husk biomass: Analysis of its biochar properties. *Energy Sources, Part A: Recovery, Utilization, and Environmental Effects*, 39(8), 761–767. <https://doi.org/10.1080/15567036.2016.1263252>
 49. Tang, Z., Chen, Y., Liu, J., Cheng, W., Wang, X., Hu, Q., Yang, Y., Yang, H., Chen, H. (2024). Study of the interaction mechanism between the components of microalgae by thermal behaviors and pyrolysis characteristics. *Journal of Analytical and Applied Pyrolysis*, 177, 106333. <https://doi.org/10.1016/j.jaap.2023.106333>
 50. Tayibi, S., Monlau, F., Fayoud, N., Oukarroum, A., Zeroual, Y., Hannache, H., Barakat, A. (2019). One-pot activation and pyrolysis of Moroccan Gelidium sesquipedale red macroalgae residue: production of an efficient adsorbent biochar. *Biochar*, 1(4), 401–412. <https://doi.org/10.1007/s42773-019-00033-2>
 51. Tsarpali, M., Kuhn, J. N., Philippidis, G. P. (2024). Activated carbon production from algal biochar: Chemical activation and feasibility analysis. *Fuel Communications*, 19(April), 100115. <https://doi.org/10.1016/j.jfueco.2024.100115>
 52. Yadav, M., Thakore, S., Jadeja, R. (2022). Removal of organic dyes using *Fucus vesiculosus* seaweed bioadsorbent an ecofriendly approach: Equilibrium, kinetics and thermodynamic studies. *Environmental Chemistry and Ecotoxicology*, 4(December 2021), 67–77. <https://doi.org/10.1016/j.enceco.2021.12.003>
 53. Yao, X., Ji, L., Guo, J., Ge, S., Lu, W., Cai, L., Wang, Y., Song, W., Zhang, H. (2020). Magnetic activated biochar nanocomposites derived from wakame and its application in methylene blue adsorption. *Bioresource Technology*, 302(November 2019), 122842. <https://doi.org/10.1016/j.biortech.2020.122842>
 54. Yu, J., Tobilko, V. (2024). Removal of methylene blue from water by NiO-modified silica gel. *Technology Audit and Production Reserves*, 6(3(80)), 47–52. <https://doi.org/10.15587/2706-5448.2024.319822>
 55. Zahara, Z. A., Royani, I., Palapa, N. R., Mohadi, R., Lesbani, A. (2023). Treatment of methylene blue using Ni-Al/Magnetite biochar layered double hydroxides composite by adsorption. *Bulletin of Chemical Reaction Engineering & Catalysis*, 18(4), 659–674. <https://doi.org/10.9767/bcrec.20049>
 56. Zou, X., Zhai, M., Liu, G., Wang, T., Guo, L., Zhang, Y., Liaquat, R. (2024). In-depth understanding of the microscopic mechanism of biochar carbonaceous structures during thermochemical conversion: Pyrolysis, combustion and gasification. *Fuel*, 361(November 2023), 130732. <https://doi.org/10.1016/j.fuel.2023.130732>